Journal of Geophysical Research: Oceans

Supporting Information for

Long-term Trends in Chesapeake Bay Remote Sensing Reflectance: Implications for Water Clarity

Jessica S. Turner[1 2], Carl T. Friedrichs[1], and Marjorie A. M. Friedrichs[1]

[1]Virginia Institute of Marine Science, William & Mary, Gloucester Point, VA, USA

[2]Department of Marine Sciences, University of Connecticut Avery Point, Groton, CT, USA (Current affiliation)

Corresponding author: Jessica S. Turner (jturner@uconn.edu)

Contents of this file

Introduction

The supporting information in this file includes: skill metric calculations for validation of satellite Rrs (Text S1), explanation of the effect of spatial resolution (Text S2), explanation of Figure S10 (Text S3), explanation of seasonal adjustment (Text S4), illustrations of the number of points included in monthly composite images (Figures S1, S2, S3), temporal distribution of the validation dataset (Figure S4), further information on validation (Figure S5), effect of spatial resolution on long-term trends (Figures S6 and S7), example red-band remote sensing reflectance spatial patterns by month (Figure S8), seasonally adjusted trend maps for single bands (Figure S9) and band ratios (Figure S10), seasonal long-term trends in example single band Rrs (Figure S11) and example band ratios (Figure S12), streamflow (Figure S13), example red-band remote sensing reflectance spatial pattern by year (Figure S14), background information on other studies using MODIS to study Chesapeake Bay water quality and their reported uncertainties (Table S1), validation statistics including multiple spatial resolutions of satellite data (Table S2), a listing of previously used algorithms relevant to this study (Table S3), and a comparison of seasonally-adjusted results to original results for single band Rrs (Table S4) and band ratios (Table S5).

Text S1.

Mean ratio, bias, mean absolute error (MAE), root mean squared error (RMSE), and mean absolute percent difference (mean APD) are calculated as:

$$Mean\ ratio = \frac{mean_{satellite}}{mean_{in\ situ}} \quad (1)$$

$$Bias = mean_{satellite} - mean_{in\ situ} \quad (2)$$

$$MAE = \frac{\sum_{i=1}^{n} |satellite_i - in\ situ_i|}{n} \quad (3)$$

$$RMSE = \sqrt{\frac{\sum_{i=1}^{n} (satellite_i - in\ situ_i)^2}{n}} \quad (4)$$

$$Mean\ APD\ (\%) = \frac{\sum_{i=1}^{n} (|satellite_i - in\ situ_i| \ / \ in\ situ_i)}{n} * 100 \quad (5)$$

where n is the number of matchup points and $satellite_i$ and $in\ situ_i$ are the ith of the respective data points.

Text S2.

For trends in Rrs(469), Rrs(555), and Rrs(645), spatial resolutions (500 m vs. 1 km for 469 and 555 nm; 250 m vs. 500 m vs. 1 km for 645 nm) marginally influenced the magnitude of long-term trends, but not enough to markedly influence results (Figure S9). In short, a decrease over time was found for Rrs in the upper Bay and in some tributaries, especially at 469 nm, while an increase over time was found for the lower Bay Rrs, particularly at the green wavelengths (488, 531, 547, and 555 nm). The use of different spatial resolutions for analysis slightly influenced resulting temporal trends in band ratios, but never changed their sign. For Rrs(645)/Rrs(555), the median trends were -0.002 and -0.0019 yr^{-1} for 1 km and 500 m spatial resolutions, respectively. For Rrs(555)/Rrs(469), the median trends were 0.0028 yr^{-1} and 0.0024 yr^{-1} for 1 km and 500 m resolutions. Although the absolute magnitudes of both trends were slightly greater for the 1 km spatial resolution, both the long-term decrease in Rrs(645)/(555) and the long-term increase in Rrs(555)/Rrs(469) were found to be similar in magnitude and similarly meaningful at 1 km vs. 500 m resolutions (Figure S10).

Text S3.

Results showed seemingly contradictory findings for single bands vs. associated ratios. Substantial trends in band ratios sometimes resulted from opposing trends in Rrs(λ), even if opposing single-band Rrs(λ) trends were small in magnitude or not meaningful. For example, for the red-to-blue ratio Rrs(645)/Rrs(488), a strong decrease over time was found in the lower Bay (Figure 4i). In some locations, this strong decrease was associated with a slight increase in Rrs(488) corresponding with a negligible, not meaningful decrease in Rrs(645) such as at the station located just south of Tangier Island in the eastern lower Bay, where a decreasing trend over time is observed in Rrs(645)/Rrs(488) (Figure S11).

Text S4.

For comparison, the long-term trend analysis was performed on Rrs and band ratio time series that had first been seasonally adjusted. Differences between the original analysis and seasonally-adjusted analysis were generally very small. For example, the spatial distribution of significant trends shifted slightly for each band (Figure S13) and each band ratio (Figure S14).

For single band Rrs trends (Table S4), seasonally adjusted results were very close to the original results presented in the main text of the paper. Differences included slightly larger spatial extent of increasing trends after de-seasonalizing (+3% to +7% spatially), slightly larger or the same spatial extent of decreasing trends after de-seasonalizing (+1% spatially at most), smaller magnitude absolute change and slightly smaller relative change of increasing trends (less than 0.1% in terms of difference between original and de-seasonalized), and very slightly smaller magnitude absolute change and relative change of decreasing trends after seasonalizing (negligible difference in either sr^{-1} yr^{-1} or % yr^{-1}).

For band ratio trends (Table S5), seasonally adjusted results were also very close to the original results presented in the main text of the paper. In terms of absolute magnitude of trends, most values were less than 0.001 yr-1 different between the original and seasonally adjusted analyses. For two green to blue ratios, seasonally adjusted trends were slightly smaller in magnitude than the original trends: for Rrs(555)/Rrs(469) and Rrs(547)/Rrs(469) showed differences of 0.002 yr-1and 0.004 yr-1 respectively. In terms of relative trends, differences between original and seasonally adjusted trends were negligible (less than 0.2% for all band ratios). Spatial extents of significant trends were slightly larger after seasonal adjustment (generally 1 to 3% more spatial coverage). For two green to blue ratios, seasonally adjusted trends were significant over a slightly larger spatial extent of the Bay than the original trends: for Rrs(555)/Rrs(469) and Rrs(547)/Rrs(469), increasing trends were significant over 7% more and 6% more than the original spatial extents, respectively.

Overall, these differences were not substantial enough to merit replacing the analysis with the seasonally adjusted analysis. Comparisons of results are provided in Tables S4 and S5. Trend maps for comparison are provided in Figures S14 and S15.

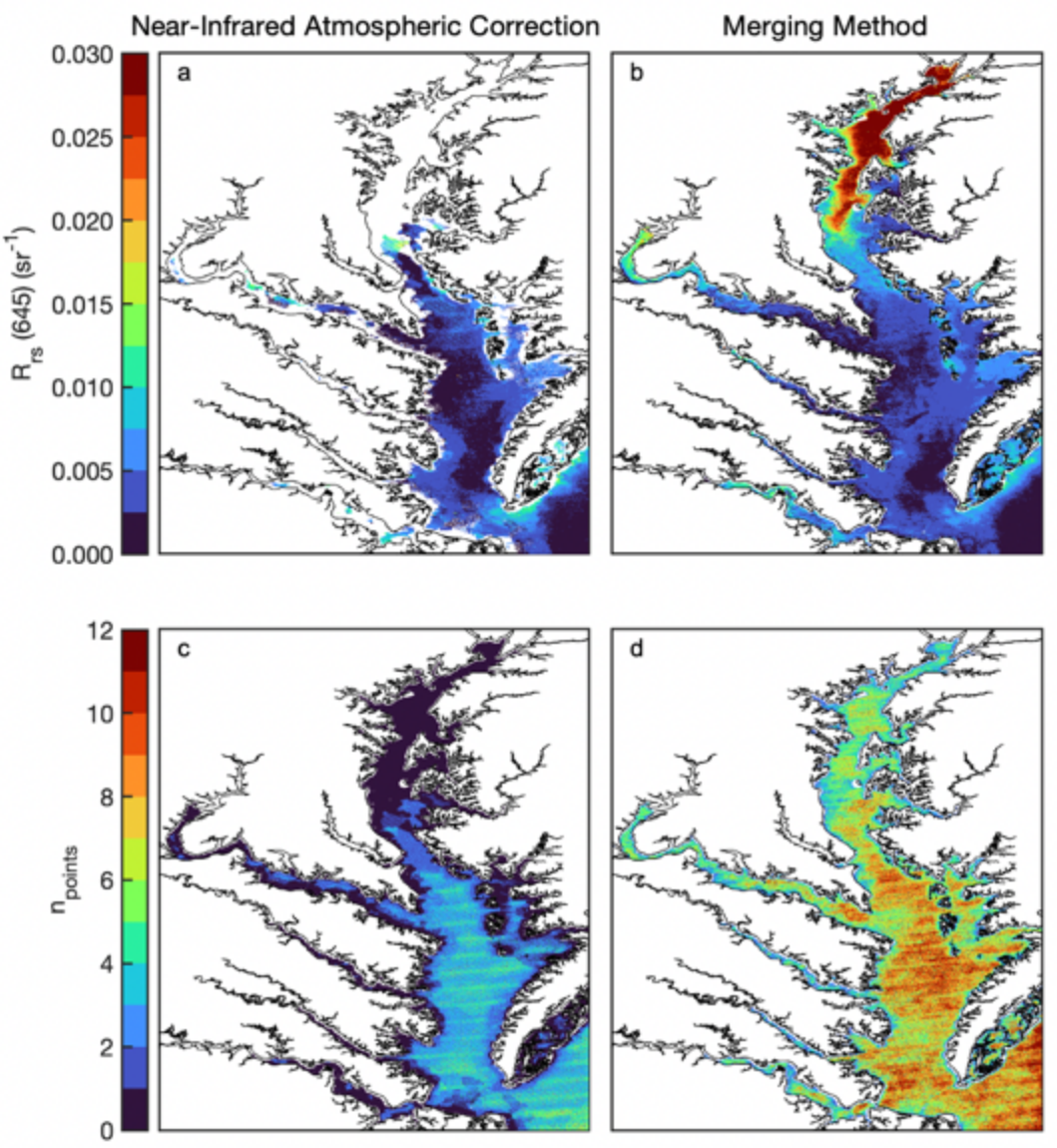

Figure S1. Data retention by the merging method for atmospheric correction, shown by an example monthly composite image, including **a,b)** Rrs(645) and **c,d)** number of scenes pixel-by-pixel (n_{points}) used in the monthly composite: **a,c)** with near-infrared atmospheric correction vs. **b,d)** with the merging method for atmospheric correction used in this study. The example shown is September 2011, a highly turbid month following large storm events.

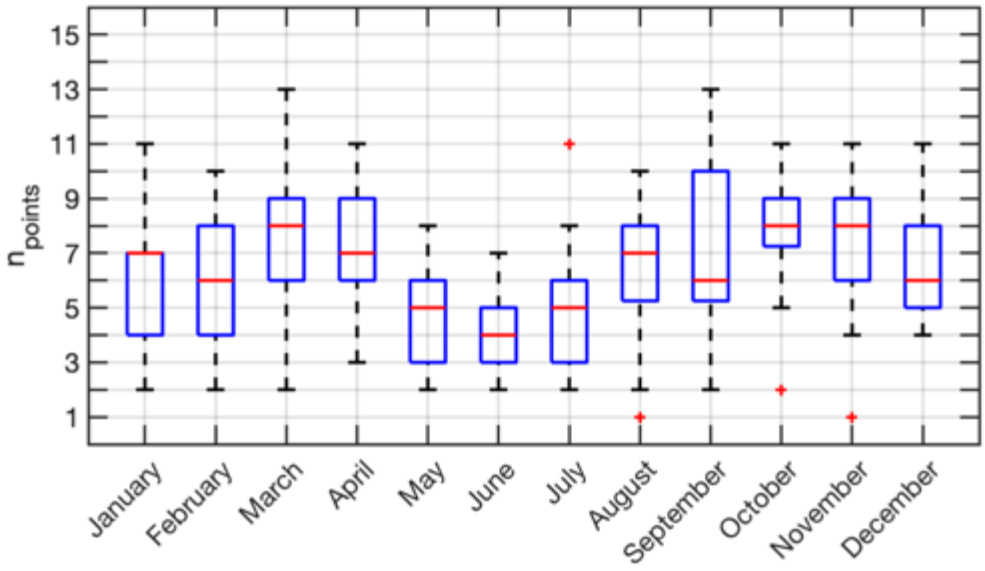

Figure S2. Climatology of the number of points used in MODIS-Aqua monthly composite scenes 2003-2020, a proxy for number of cloud-free daily scenes per month. n_{points} represents the spatial median of the number of points used to create each monthly composite scene, and each month's boxplot indicates the median (red lines), upper quartile, and lower quartile (top and bottom of blue boxes) of the spatial medians for that month over all years.

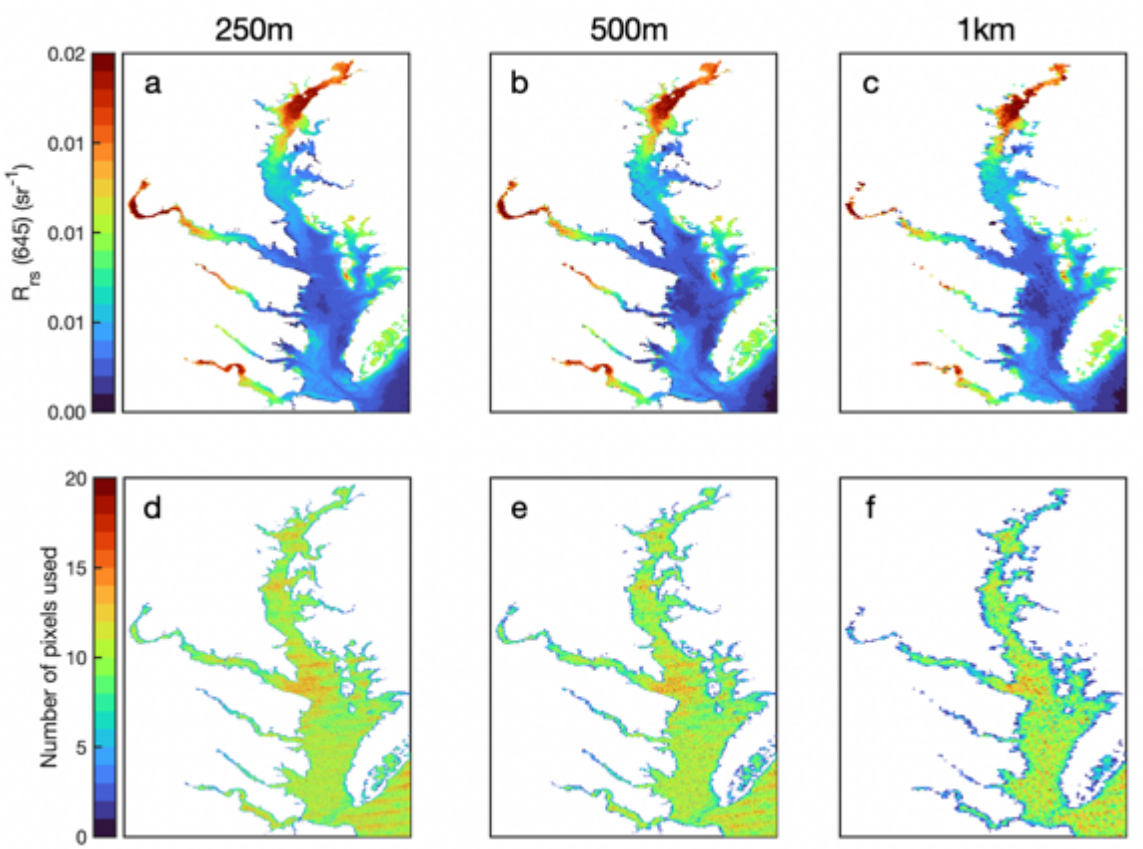

Figure S3. Effects of spatial resolution on data quantity in monthly composites, including **a-c)** monthly composite Rrs 645 (sr^{-1}) and **d-f)** number of points contributing to monthly composite scenes (n_{points}) for **a, d)** 250 m, **b, e)** 500 m, and **c, f)** 1 km spatial resolutions during the example month March 2011. Spatial median n_{points} for the three lower subplots are, from left to right, 9, 8, and 8 points.

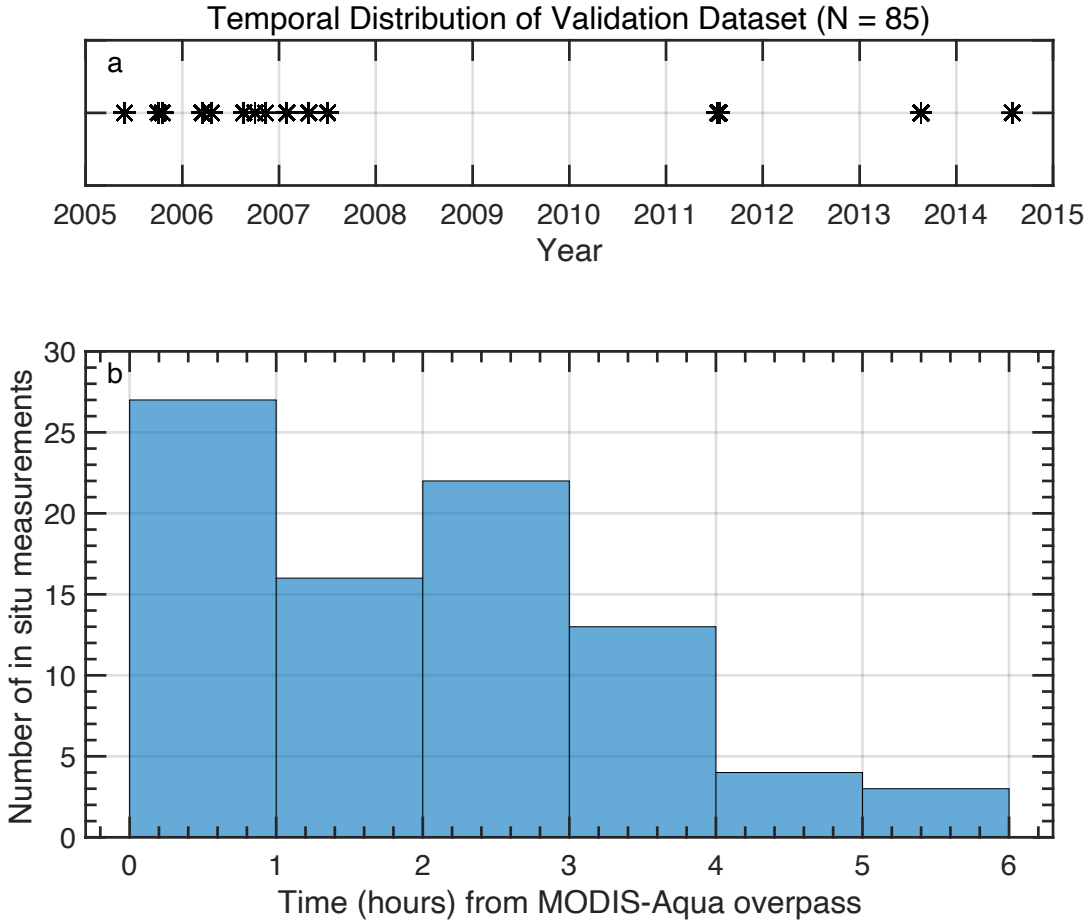

Figure S4. Temporal distribution of the validation dataset (N = 85), including **a)** distribution over the years 2005 through 2014 and **b)** timing of in situ Rrs measurement matchups in number of hours from MODIS-Aqua overpass on each day.

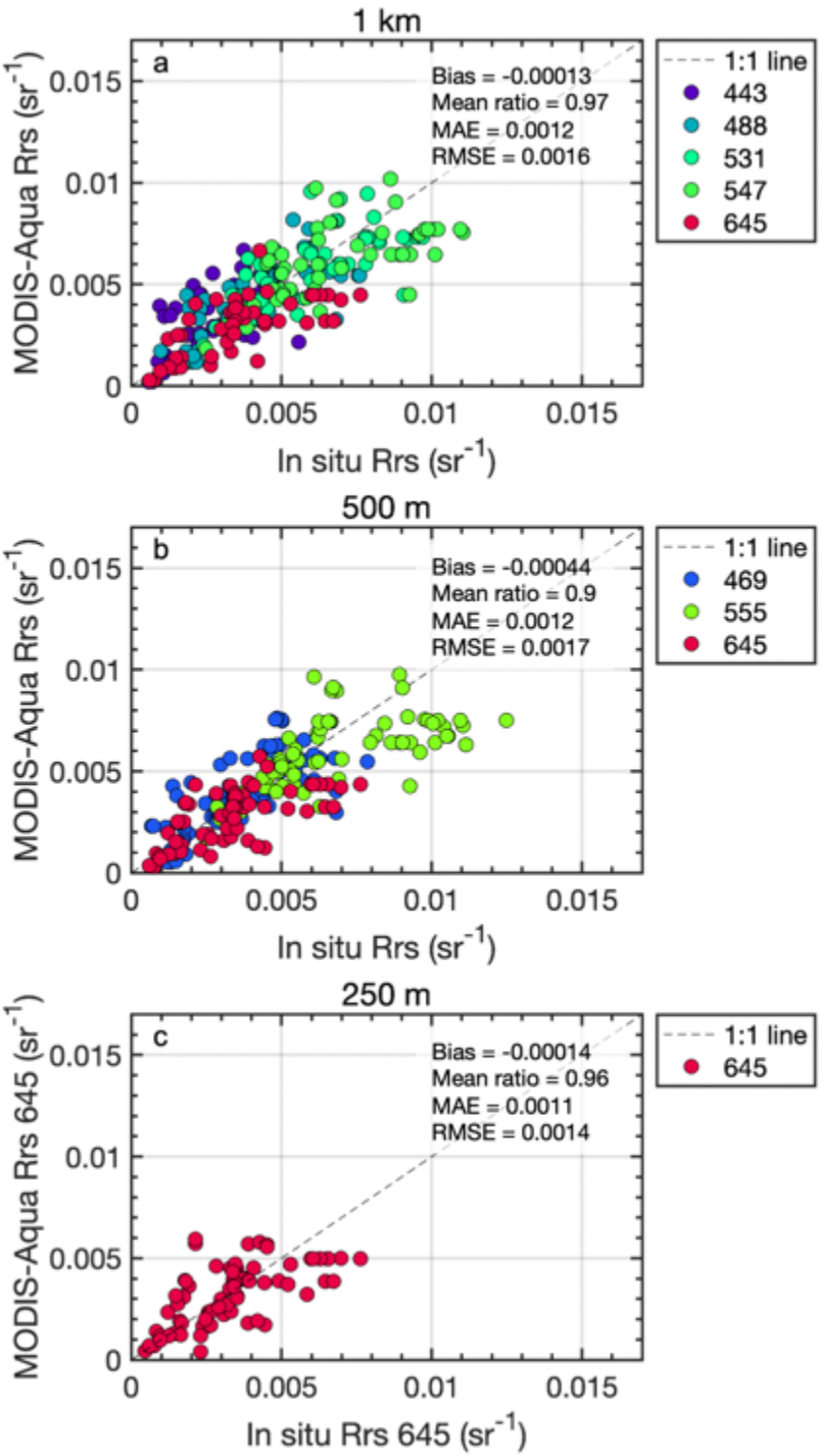

Figure S5. Validation at all spatial resolutions of MODIS-Aqua Rrs(λ) with in situ Rrs(λ) observations, for: **a)** 1 km ("standard" ocean color) spatial resolution retrievals of Rrs(λ) using 1-pixel spatial matchup window, **b)** 500 m (HKM) spatial resolution retrievals of Rrs(λ) using 3x3 pixel matchup window, and **c)** 250 m (QKM) spatial resolution retrievals of Rrs(645) using 5x5 pixel matchup window. For skill of individual Rrs(λ) bands, see Table S4.

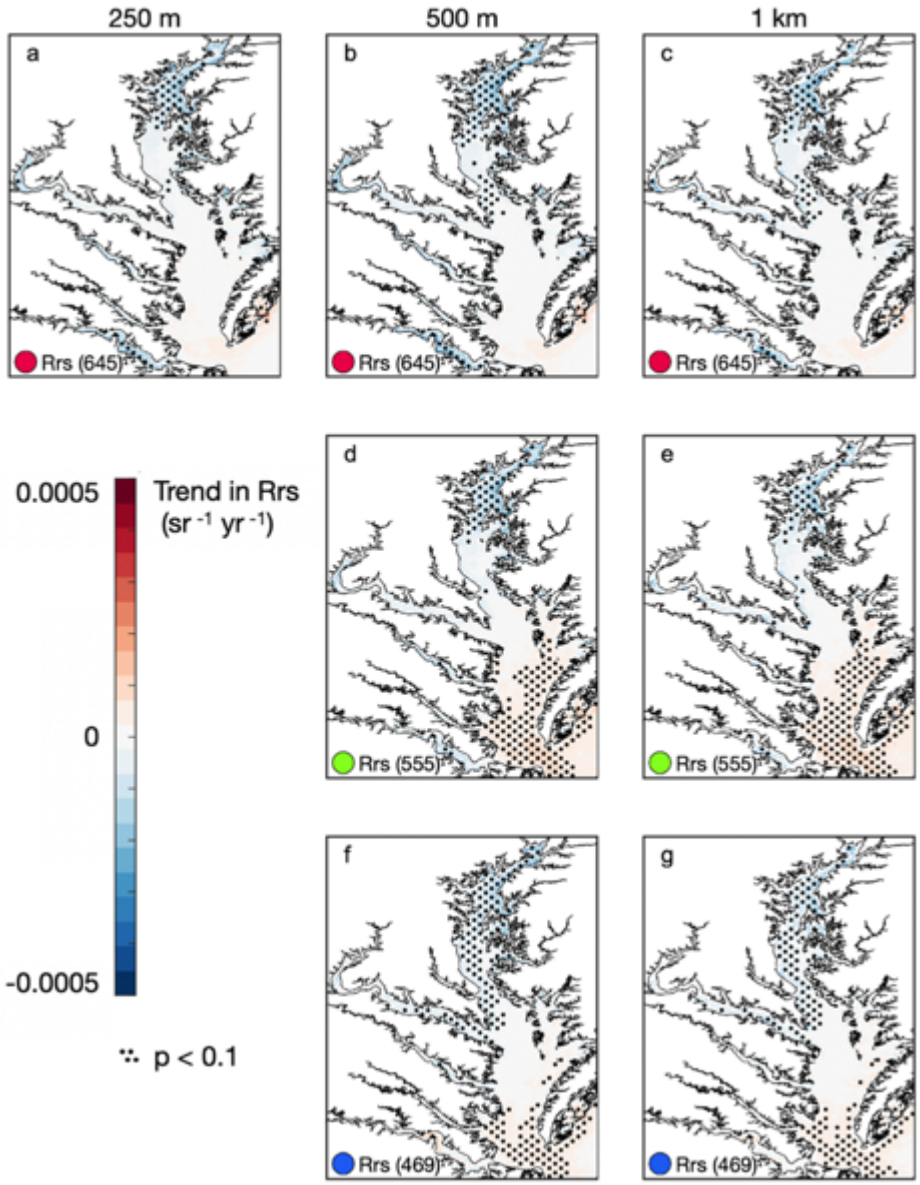

Figure S6. Comparison of single-band Rrs trends for higher spatial resolution bands. **a-c)** red band Rrs(645), **d,e)** green band Rrs(555), and **f,g)** blue band Rrs(469), at **a)** 250 m, **b,d,f)** 500 m vs. **c,e,g)** 1 km spatial resolution.

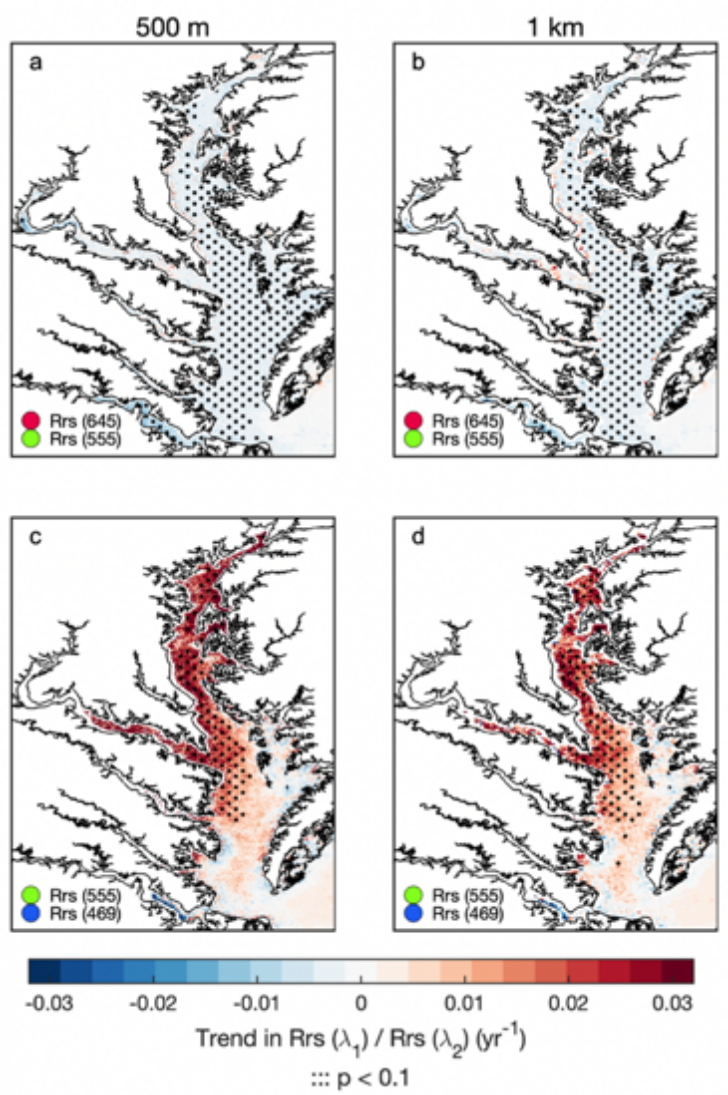

Figure S7. Comparison of Rrs band ratio trends for higher spatial resolution bands. **a,b)** red-to-green ratio Rrs(645)/Rrs(555) and **c,d)** green-to-blue ratio Rrs(555)/Rrs(469), at **a,c)** 500 m vs. **b,d)** 1 km spatial resolution.

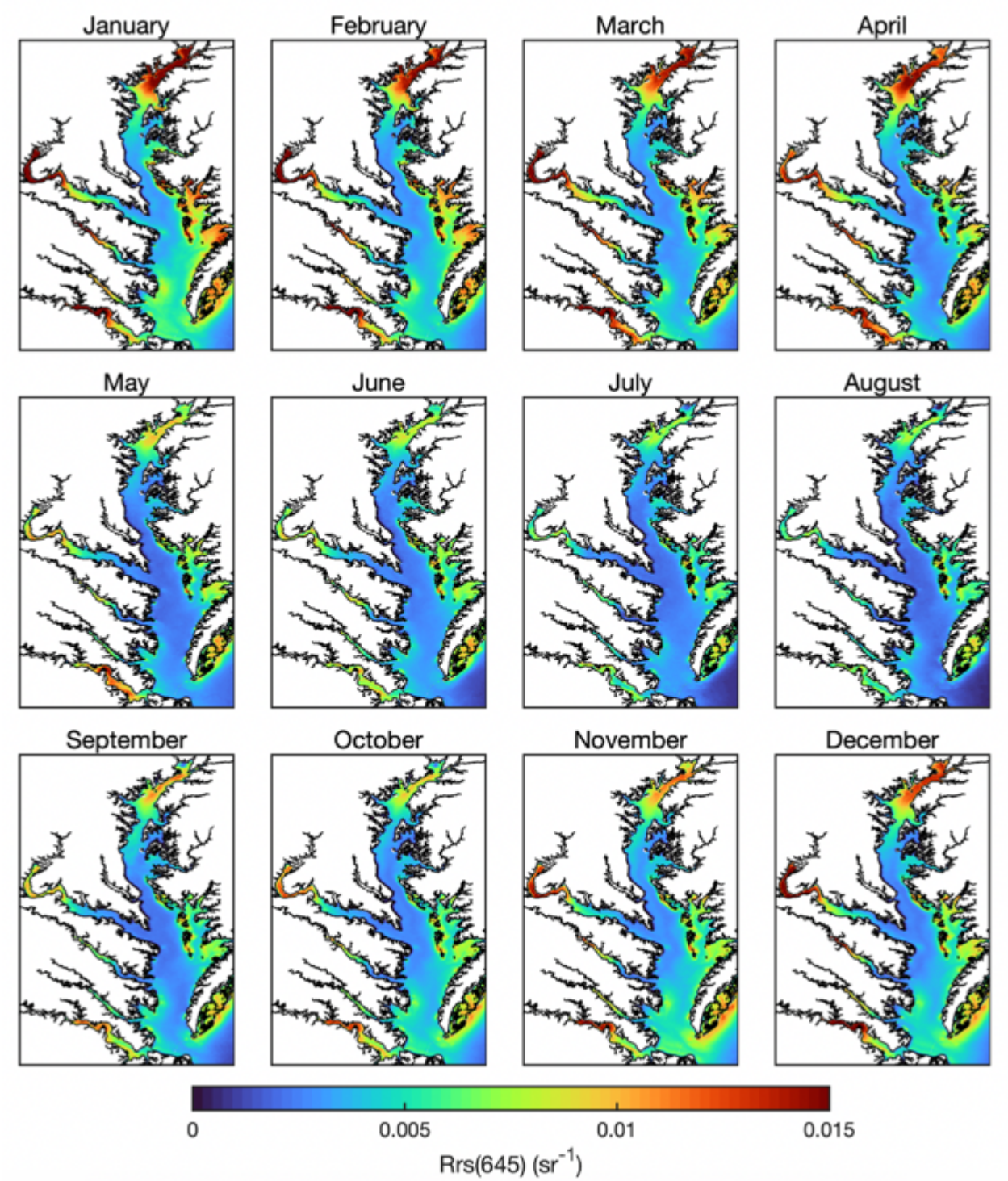

Figure S8. Monthly mean Rrs(645) (sr^{-1}) for the Chesapeake Bay 2003 to 2020 at 250 m nominal spatial resolution.

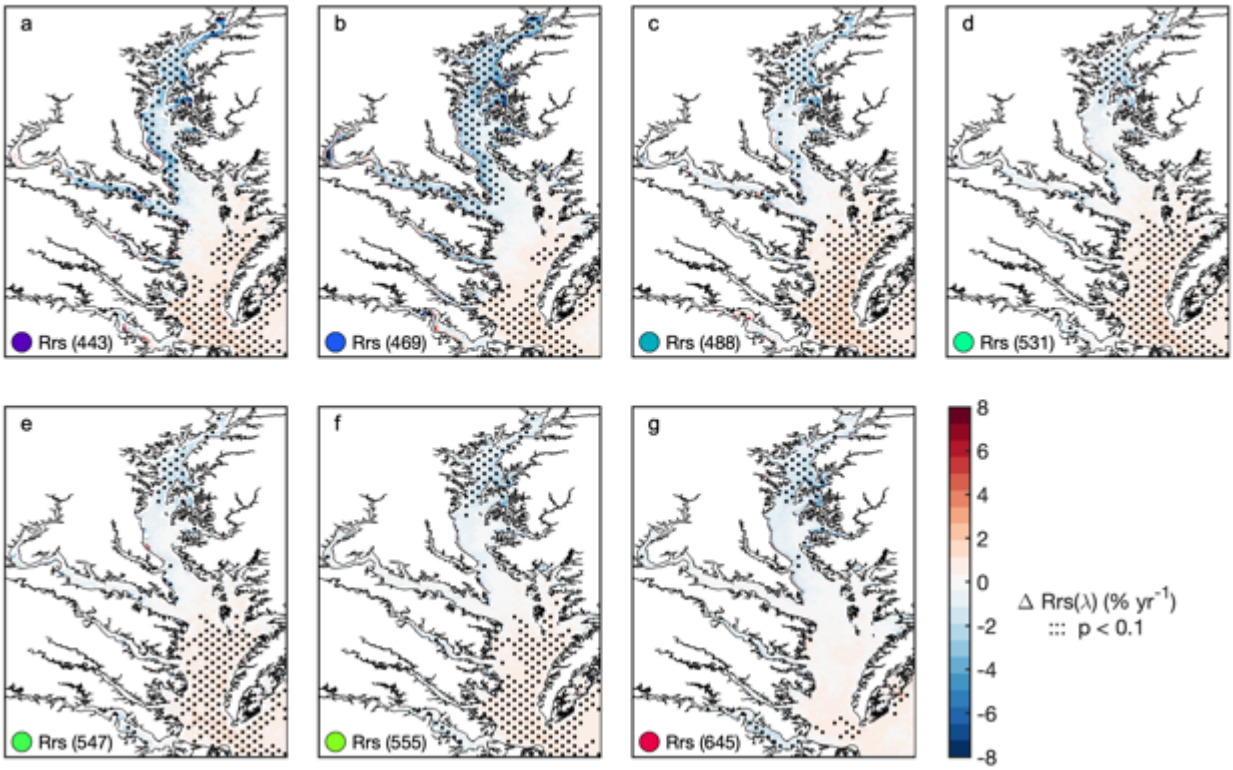

Figure S9. Seasonally adjusted trends over time in Rrs at single bands, from 2003 to 2020 for bands **a)** 443 nm through **g)** 645 nm according to linear least-squares fits over all surface water areas with > 80% of monthly images at the nominal spatial resolution of each band, i.e., **g)** Rrs(645) at 250 m, **b)** Rrs(469) and **f)** Rrs(555) at 500 m, and all other bands at 1 km. Small black dots highlight significant trends ($p < 0.1$). Trends are expressed as relative trends normalized to the long-term mean Rrs at each location (% yr^{-1}). Absolute values of median increasing and decreasing trends over time were 0.7 to 0.9% yr^{-1} and 1.3 to 2.8% yr^{-1}, respectively (see Table S4).

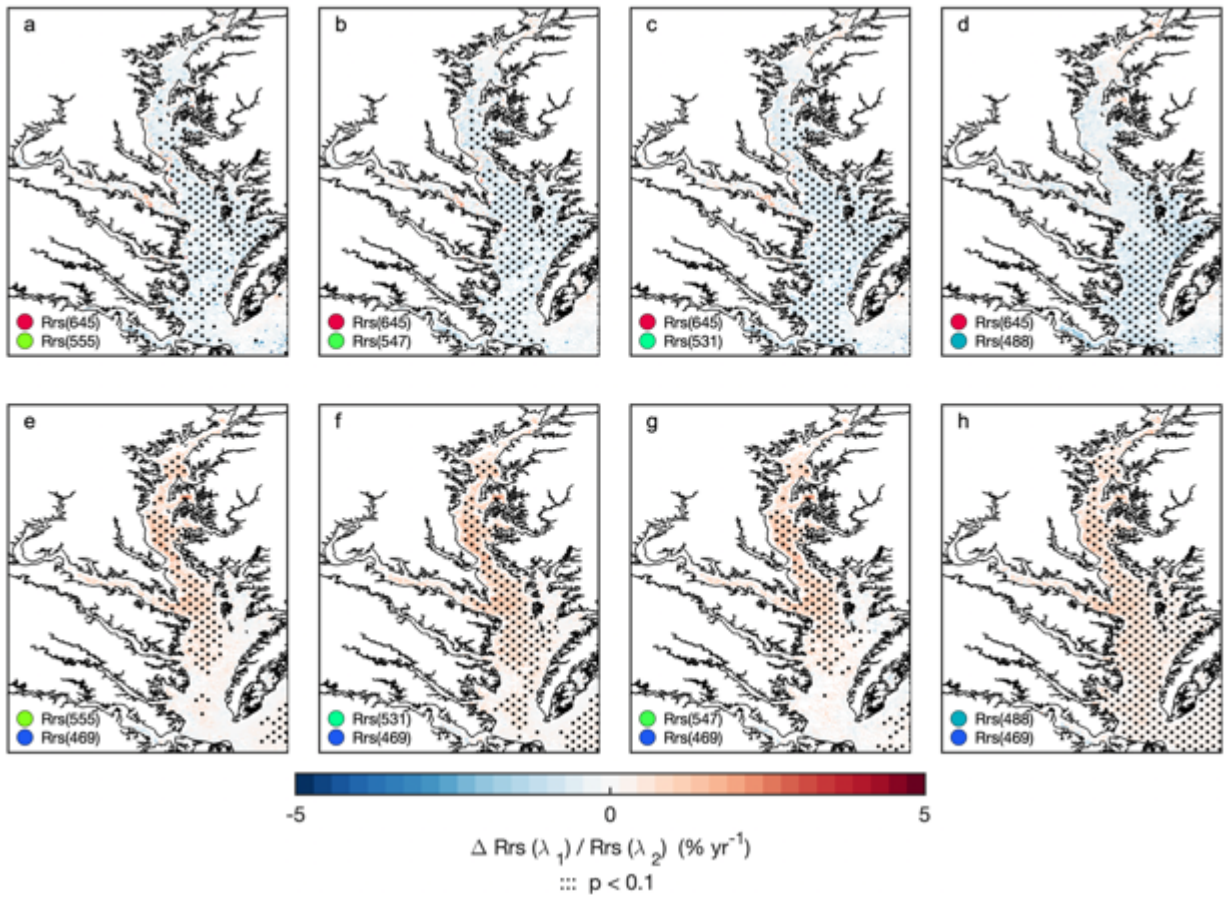

Figure S10. Seasonally adjusted trends over time 2003-2020 in selected band ratios ($Rrs(\lambda_1)/Rrs(\lambda_2)$), including **a-c)** decreasing red-to-green ratios, **d)** a decreasing red-to-blue ratios, and **e-h)** increasing green-to-blue ratios. Selected trends shown were > +/- 0.003 yr^{-1} in magnitude and significant ($p < 0.1$) for > 15% of the Bay. Trends are expressed as relative trends normalized to the long-term mean value at each location (% yr^{-1}). Absolute values of median trends ranged from 0.5 to 0.8% yr^{-1}, respectively (see Table S5).

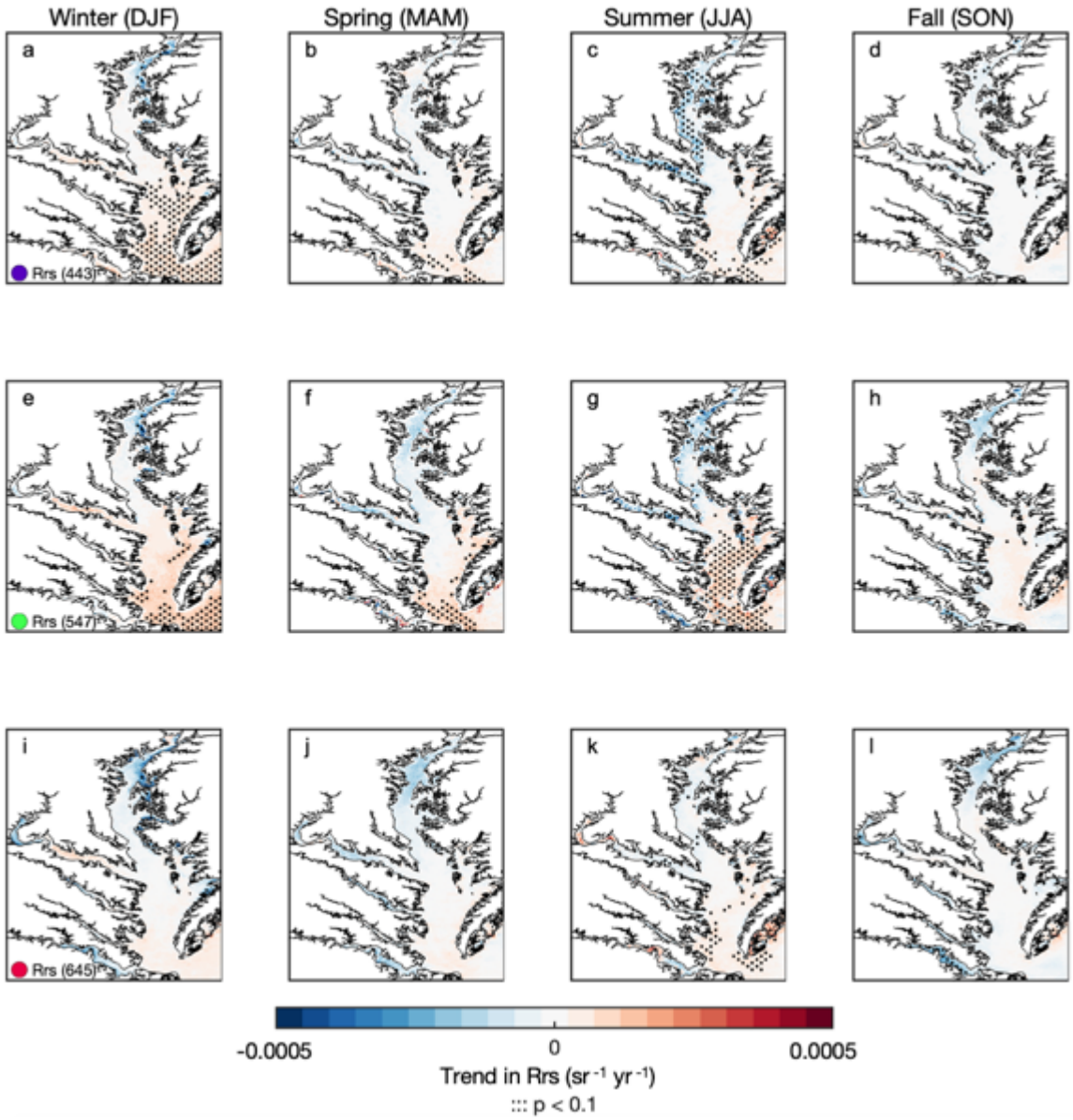

Figure S11. Example seasonal trends 2003-2020 for three single bands, including **a-d)** blue band Rrs(443), **e-h)** green band Rrs(547), and **i-l)** red band Rrs(645). Seasons include **a,e,i)** winter (December-February), **b,f,j)** spring (March-May), **c,g,k)** summer (June-August), and **d,h,l)** fall (September-November). Small black dots indicate regions where linear trends were most substantial ($p < 0.1$).

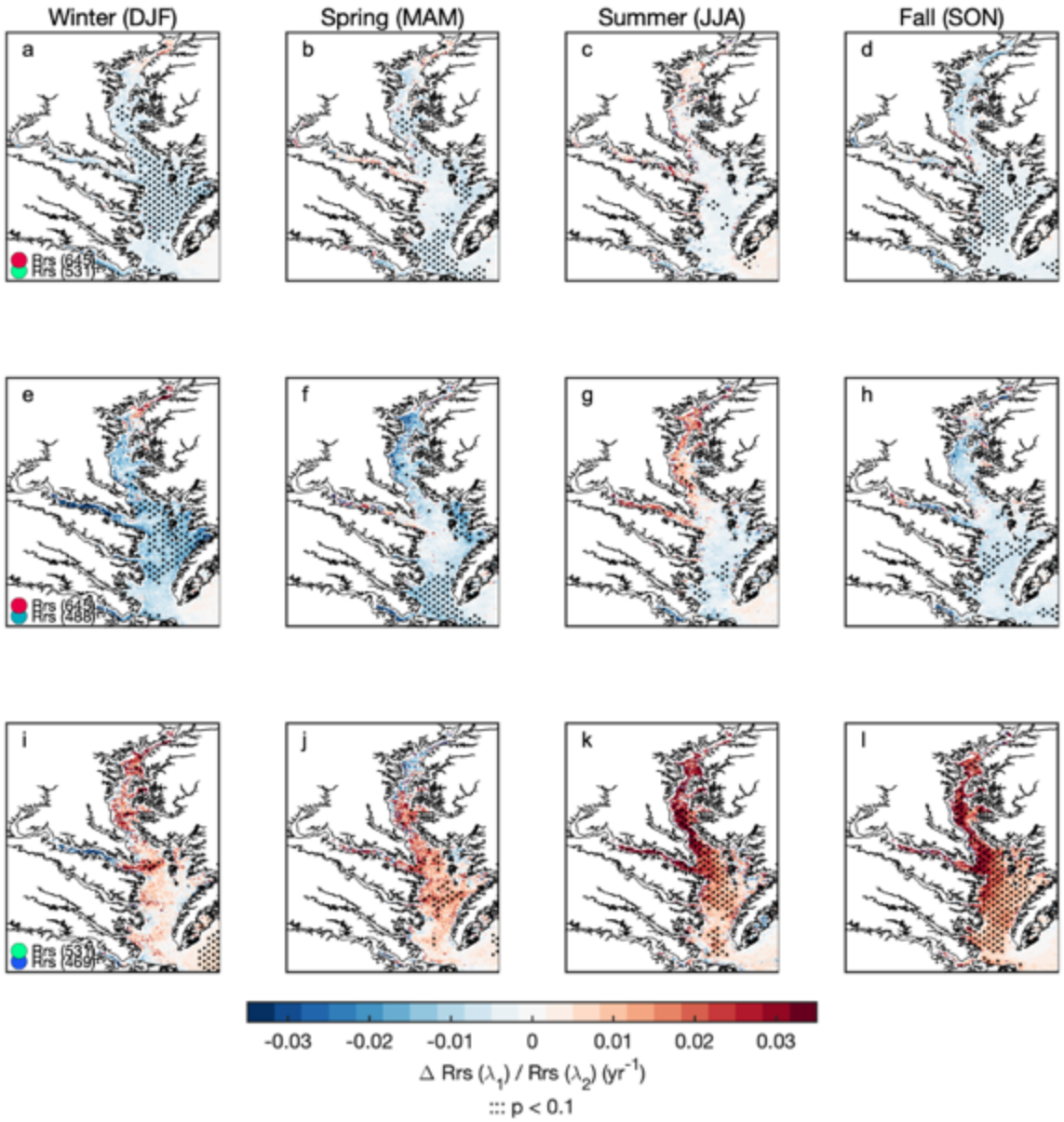

Figure S12. Example seasonal trends 2003-2020 for three band ratios including **a-d)** red-to-green ratio Rrs(645)/Rrs(531), **e-h)** red-to-blue band ratio Rrs(645)/Rrs(488), and **i-l)** green-to-blue band ratio Rrs(531)/Rrs(469), including seasons **a,e,i)** winter (December-February), **b,f,j)** spring (March-May), **c,g,k)** summer (June-August), and **d,h,l)** fall (September-November). Small black dots indicate regions where linear trends were most substantial ($p < 0.1$).

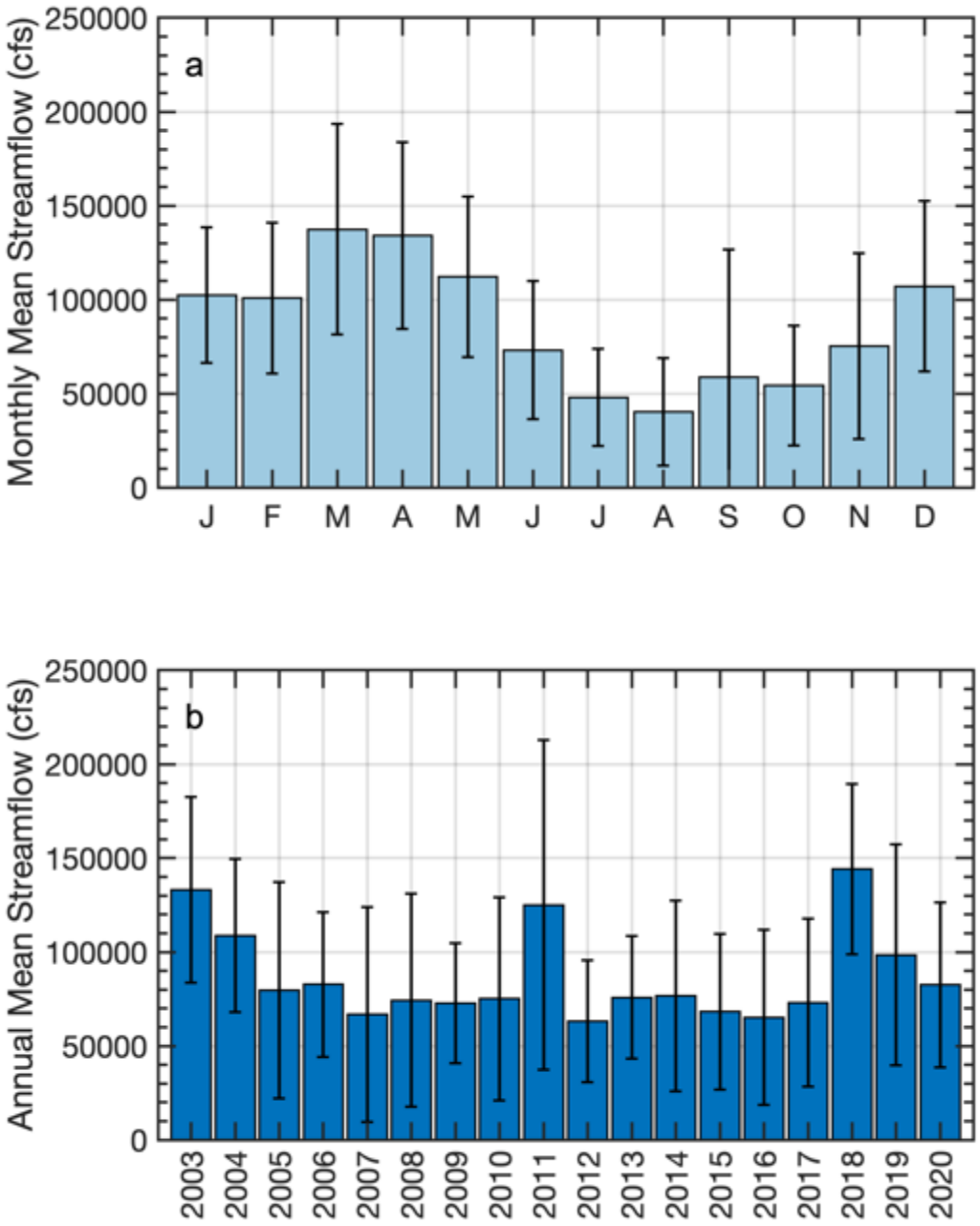

Figure S13. Mean streamflow to the Chesapeake Bay 2003 to 2020 from the three major rivers (Susquehanna, Potomac, and James Rivers) in cubic feet per second (cfs). **a)** Monthly mean streamflow; error bars represent standard deviation among years**. b)** Annual mean streamflow; error bars represent standard deviation among months. Data courtesy of the United States Geological Survey (USGS). https://www.usgs.gov/centers/cba/science/freshwater-flow-chesapeake-bay?qt-science_center_objects=0#qt-science_center_objects

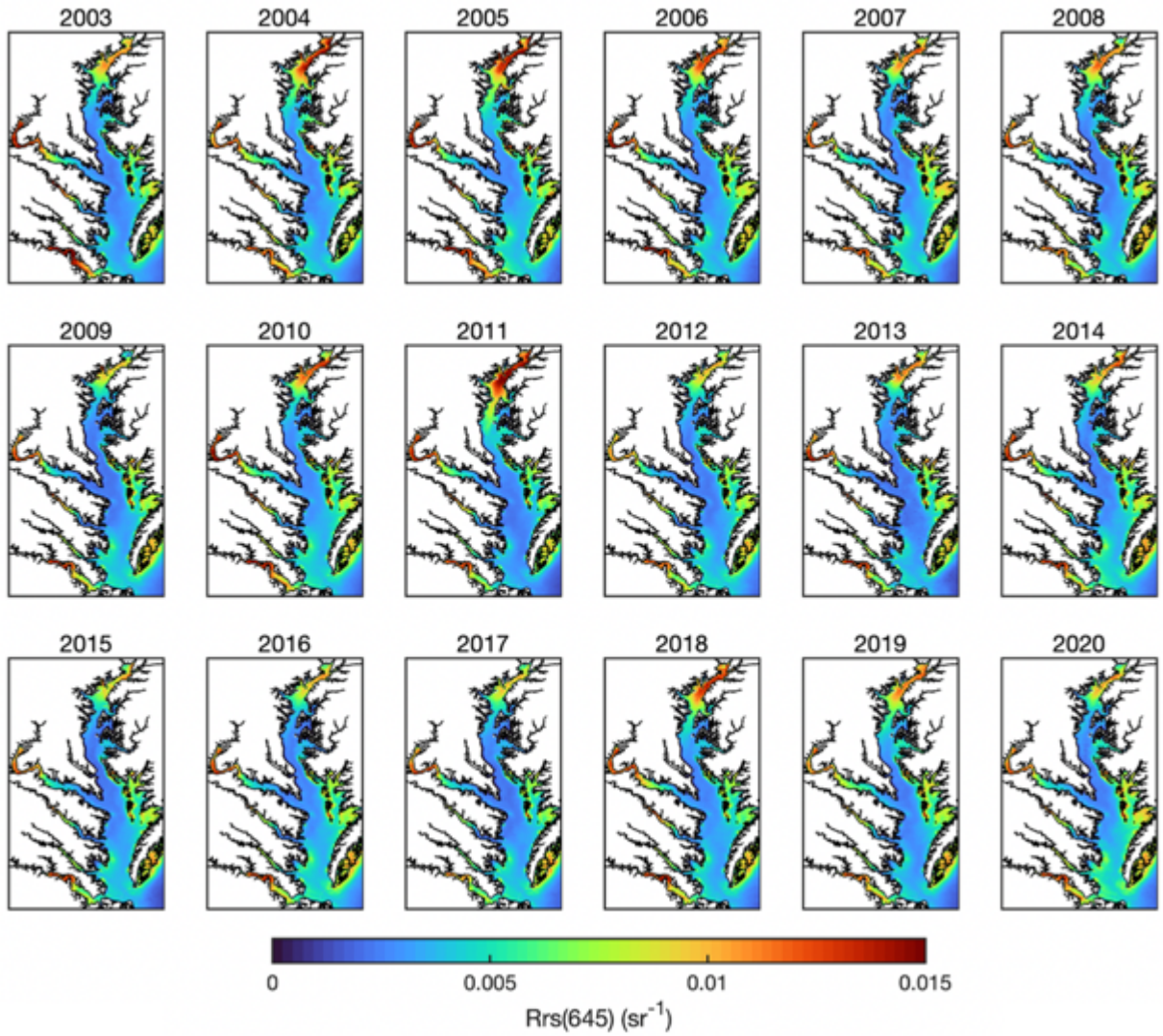

Figure S14. Annual mean Rrs(645) (sr^{-1}) for the Chesapeake Bay 2003 to 2020 at 250 m nominal spatial resolution.

Table S1. Past MODIS-Aqua retrievals in Chesapeake Bay with uncertainties.

Study	**Variable**	**Metric***	**Uncertainty**†
Wang et al. (2009)	K_d	Mean ratio	0.96
Hasan & Benninger (2017)	TSS	Mean ratio	1.052
		Mean APD	46.21%
		R^2	0.91
Ondrusek et al. (2012)	TSS	R^2	0.79 to 0.90
DeLuca et al. (2018)	TSS	MAE	2.38 to 2.97 mg L^{-1}
		RMSE	4.3 to 5.61 mg L^{-1}
Zheng et al. (2015)	TSS	R	0.71
		RMSE	4 mg L^{-1}
Son & Wang (2012)	TSS	Mean ratio	1.06
		Median ratio	0.97
	nLw(λ)	Mean ratio	0.87 to 1.29
	Chl-a	Mean ratio	1.4
Werdell et al. (2009)	Chl-a	Mean ratio	0.88 to 1.69
		Mean APD	69.3 to 40.1%
Le et al. (2013)	Chl-a	Mean ratio	1.09
		R^2	0.43
Mannino et al. (2008)	a_{CDOM}(443)	RMSE	0.015 to 0.04 m^{-1}
		Mean APD	11 to 25%
Cao et al. (2018)	a_{CDOM}(300)	RMSE	0.9 m^{-1}
		Mean APD	36%
		Percent bias	-5%
Signorini et al. (2019)	DOC	RMSE	23.9 μmol L^{-1}
		Bias	-21.2 μmol L^{-1}
This study	Rrs(λ)	Mean ratio	0.8 to 1.4
		Bias	-0.0009 to 0.0006 sr^{-1}
		Mean APD	1 to 37%
		R	0.58 to 0.75

*MAE = maximum absolute error, RMSE = root mean squared error, R = correlation coefficient, APD = absolute percent difference.

†Values are reported for single variables, and ranges are reported if multiple wavelengths or multiple algorithms were investigated.

Table S2. Validation of satellite Rrs including multiple spatial resolutions.

Spatial resolution	λ (nm)	n*	Mean ratio	Bias (sr^{-1})	MAE † (sr^{-1})	RMSE † (sr^{-1})	Mean APD †	R †
1 km	443	63	1.1	0.0003	0.0010	0.0014	12%	0.67
	488	63	1.0	0.00004	0.0010	0.0013	1%	0.75
	531	63	1.0	-0.0002	0.0012	0.0015	1%	0.67
	547	63	0.9	-0.0007	0.0015	0.0020	7%	0.61
	645	63	0.8	-0.0007	0.0012	0.0015	15%	0.70
500 m	469	81	1.1	0.0002	0.0010	0.0014	15%	0.73
	555	81	0.9	-0.0009	0.0016	0.0021	9%	0.60
	645	81	0.8	-0.0006	0.0011	0.0015	12%	0.66
250 m	645	85	1.0	-0.0001	0.0011	0.0014	6%	0.65

*Paired data points using in situ observed Rrs(λ) vs. corresponding daily (<6 hours) MODIS-Aqua pixels or pixel window averages.

† MAE = Mean absolute error, RMSE = Root mean squared error, Mean APD = Mean absolute percent difference, and R = correlation coefficient (See Supporting Information Text S1 for calculations).

Table S3. Relevant empirical algorithms for satellite-derived water clarity products.

Product	Most relevant band or band ratio	References
Chl-a concentration	Green-to-blue	O'Reilly et al. (1998) Werdell et al. (2009)*
	Red-to-green*	Tzortziou et al. (2007) Le et al. (2013) Ioannou et al. (2014) Abbas et al. (2019)
Chl-a fluorescence	Red-edge fluorescence line height	Letelier & Abbot (1996) Abbott & Letelier (1999) Huot et al. (2005)
	NIR-to-red*	Gitelson et al. (2007) Ioannou et al. (2014) Gilerson et al. (2015)
TSS	Red	Nechad et al. (2010) Ondrusek et al. (2012)* Constantin et al. (2016) Hasan & Benninger (2017)* DeLuca et al. (2018)* Tavora et al. (2019)
	Red-to-green	Qiu et al. (2017) Reisinger et al. (2017)
	Red-to-blue	Son & Wang (2012)* Liu & Wang (2014)* Siswanto et al. (2011)
	NIR (highly turbid waters)	Doxaran et al. (2003)
Turbidity	Red	Garaba et al. (2014) Dogliotti et al. (2015) Hudson et al. (2017) Tao & Hill (2019)
	Red-to-green	Wang et al. (2021)
	NIR (highly turbid waters)	Tao & Hill (2019)
$K_d(490)$	Green-to-blue (open ocean)	Austin & Petzold (1981) Morel et al. (2007)
	Red-to-blue (coastal waters)*	Wang et al. (2009) Shi et al. (2013) Tomlinson et al. (2019)
Secchi depth	Red*	Crooke et al. (2017)
aCDOM, DOC	Green-to-blue ratio*	Mannino et al. (2008) Mannino et al. (2014) Cao et al. (2018) Signorini et al. (2019)

*Empirical algorithms developed using matchups from the Chesapeake Bay and/or Mid-Atlantic Bight region.

Table S4. Single band Rrs comparison of original results and seasonally-adjusted results.

λ (nm)	Increasing Trend (sr^{-1} yr^{-1}) *		Relative Increasing Trend (yr^{-1}) ^		Increasing PercBay †		Decreasing Trend (sr^{-1} yr^{-1}) *		Relative Decreasing Trend (yr^{-1}) ^		Decreasing PercBay †	
	Orig	Seas. Adj.	Orig	Seas. Adj.	Orig	Seas. Adj.	Orig	Seas. Adj.	Orig	Seas. Adj.	Orig	Seas. Adj.
443	0.00004	0.00003	1.0%	0.9%	18%	21%	-0.00006	-0.00005	-2.9%	-2.8%	11%	12%
469	0.00004	0.00004	0.9%	0.8%	15%	18%	-0.00006	-0.00005	-2.2%	-2.2%	20%	21%
488	0.00005	0.00005	1.0%	0.9%	26%	30%	-0.00007	-0.00007	-2.0%	-2.0%	9%	8%
531	0.00006	0.00006	0.9%	0.8%	27%	31%	-0.00010	-0.00010	-1.6%	-1.6%	8%	8%
547	0.00006	0.00006	0.8%	0.8%	22%	27%	-0.00012	-0.00012	-1.6%	-1.6%	8%	8%
555	0.00006	0.00005	0.8%	0.7%	23%	30%	-0.00010	-0.00010	-1.3%	-1.3%	12%	12%
645	0.00006	0.00004	1.0%	0.8%	3%	7%	-0.00011	-0.00010	-1.5%	-1.5%	14%	14%

* Median trend 2003 to 2020 of area exhibiting significant long-term increase or decrease ($p < 0.1$).
^ Median relative trend of area exhibiting significant long-term increase or decrease, relative to the long-term mean.
†Percent of water area analyzed exhibiting significant trend ($p < 0.1$).

Table S5. Band ratios Rrs(λ_1) / Rrs(λ_2) comparison of original results and seasonally-adjusted results.

λ_1 (nm)	λ_2 (nm)	Trend (yr^{-1}) *		Relative Trend (yr^{-1}) ^		PercBay†	
		Orig	Seas. Adj.	Orig	Seas. Adj.	Orig	Seas. Adj.
645	555	-0.003	-0.003	-0.6%	-0.6%	35%	37%
645	547	-0.004	-0.003	-0.7%	-0.7%	36%	38%
645	531	-0.005	-0.004	-0.8%	-0.7%	37%	38%
645	488	-0.008	-0.007	-0.9%	-0.8%	33%	34%
555	469	0.017	0.014	0.8%	0.7%	17%	24%
531	469	0.011	0.011	0.6%	0.6%	34%	37%
547	469	0.015	0.013	0.7%	0.6%	23%	29%
488	469	0.005	0.005	0.5%	0.5%	48%	50%

* Median trend 2003 to 2020 of area exhibiting significant trend ($p < 0.1$).
^ Median relative trend of area exhibiting significant long-term trend, relative to the long-term mean.
†Percent of water area analyzed exhibiting significant trend ($p < 0.1$).

References From the Supporting Information

Abbott, M. R., & Letelier, R. M. (1999). Chlorophyll fluorescence (MODIS product number 20) (ATBD 22). Retrieved from http://oceancolor.gsfc.nasa.gov/DOCS/atbd_mod22.pdf

Austin, R. W., & Petzold, T. J. (1981). The determination of the diffuse attenuation coefficient of sea water using the Coastal Zone Color Scanner. In J. F. R. Gower (Ed.), *Oceanography from Space* (pp. 239–256). Boston, MA: Springer US. https://doi.org/10.1007/978-1-4613-3315-9_29

Dogliotti, A. I., Ruddick, K. G., Nechad, B., Doxaran, D., & Knaeps, E. (2015). A single algorithm to retrieve turbidity from remotely-sensed data in all coastal and estuarine waters. *Remote Sensing of Environment*, *156*, 157–168. https://doi.org/10.1016/j.rse.2014.09.020

Doxaran, D., Froidefond, J.-M., & Castaing, P. (2003). Remote-sensing reflectance of turbid sediment-dominated waters. Reduction of sediment type variations and changing illumination conditions effects by use of reflectance ratios. *Applied Optics*, *42*(15), 2623. https://doi.org/10.1364/ao.42.002623

Garaba, S. P., Badewien, T. H., Braun, A., Schulz, A. C., & Zielinski, O. (2014). Using ocean colour remote sensing products to estimate turbidity at the Wadden sea time series station Spiekeroog. *Journal of the European Optical Society*, *9*, 14020. https://doi.org/10.2971/jeos.2014.14020

Gitelson, A. A., Schalles, J. F., & Hladik, C. M. (2007). Remote chlorophyll-a retrieval in turbid, productive estuaries: Chesapeake Bay case study. *Remote Sensing of Environment*, *109*(4), 464–472. https://doi.org/10.1016/j.rse.2007.01.016

Huot, Y., Brown, C. A., & Cullen, J. J. (2005). New algorithms for MODIS sun-induced chlorophyll fluorescence and a comparison with present data products. *Limnology and Oceanography: Methods*, *3*(2), 108–130. https://doi.org/10.4319/lom.2005.3.108

Letelier, R. M., & Abbott, M. R. (1996). An analysis of chlorophyll fluorescence algorithms for the moderate resolution imaging spectrometer (MODIS). *Remote Sensing of Environment*, *58*(2), 215–223. https://doi.org/10.1016/S0034-4257(96)00073-9

Liu, X., & Wang, M. (2014). River runoff effect on the suspended sediment property in the upper Chesapeake Bay using MODIS observations and ROMS simulations. *Journal of Geophysical Research: Oceans*, *119*, 8646–8661. https://doi.org/10.1002/2014JC010081

Morel, A., Huot, Y., Gentili, B., Werdell, P. J., Hooker, S. B., & Franz, B. A. (2007). Examining the consistency of products derived from various ocean color sensors in open ocean (Case 1) waters in the perspective of a multi-sensor approach. *Remote Sensing of Environment*, *111*(1), 69–88. https://doi.org/10.1016/j.rse.2007.03.012

Nechad, B., Ruddick, K. G., & Park, Y. (2010). Calibration and validation of a generic multisensor algorithm for mapping of total suspended matter in turbid waters. *Remote Sensing of Environment*, *114*(4), 854–866. https://doi.org/10.1016/j.rse.2009.11.022

Qiu, Z., Xiao, C., Perrie, W., Sun, D., Wang, S., Shen, H., et al. (2017). Using Landsat 8 data to estimate suspended particulate matter in the Yellow River estuary. *Journal of Geophysical Research: Oceans*, *122*, 276–290. https://doi.org/10.1002/2016JC012412